

Research Paper

Analysis of Scattering Light Transport in Translucent Media

YASUHIRO MUKAIGAWA,^{†1,†2} RAMESH RASKAR^{†2}
and YASUSHI YAGI^{†1}

We propose a new method to analyze scattering light transport in homogeneous translucent media. The incident light undergoes multiple bounces in translucent media, and produces a complex light field. Our method analyzes the light transport in two steps. First, single and multiple scatterings are separated by projecting high-frequency stripe patterns. Then, the light field for each bounce scattering is recursively estimated based on a forward rendering process. Experimental results show that scattering light fields can be analyzed and visualized for each bounce.

1. Introduction

Most objects in our everyday environment are not perfectly opaque, but are instead translucent. Although marble, skin, and milk are considered typical translucent objects, there are many more such objects, including fruit and vegetables. In particular, most liquids including juice and murky water are also translucent. **Figure 1** shows an example where orange juice is illuminated by a green laser beam and the incident ray scatters in the liquid. The right image is a top view of the glass in which the intensities are represented using pseudo-color. Since the incident ray undergoes repeated scattering resulting in a complex light field, we cannot directly measure a light field within a scattering medium. Understanding how an incident ray repeats the scattering and how light propagates in scattering media is fundamental for many applications including rendering, medical imaging, and material estimation.

Scattering is modeled by *single scattering* and *multiple scattering* as shown in



Fig. 1 Orange juice illuminated by a laser beam.

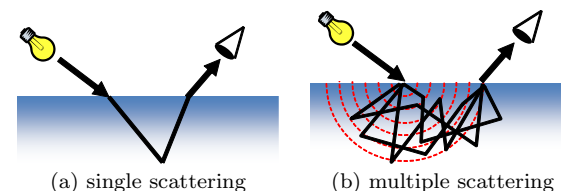


Fig. 2 Models for single and multiple scatterings.

Fig. 2. Single scattering is one bounce reflection in the media, while multiple scattering repeats reflections many times. These models have been selectively used according to the optical density. **Figure 3** shows several examples of vitamin water, orange juice and milk which have different optical densities. When these liquids are illuminated by a laser beam, obviously different spatial distributions of the scattering are observed.

In *optically thin media*, single scattering is dominant as shown in Fig. 3 (a). Several methods have been proposed to analyze single scattering. Narasimhan et al.¹⁾ estimated scattering parameters for diluted homogeneous liquid. Gu et al.²⁾ recovered inhomogeneous participating media by projecting structured light. Hawkins et al.³⁾ estimated the time-varying density of smoke using a scanning laser beam. These methods produce good results because a ray from the light source bounces only once in the media and the path of the ray is simply determined as shown in Fig. 2 (a). However, these methods can analyze only *single scattering in optically thin media*.

To deal with *optically dense media*, the spatial distribution of multiple scattering must be modeled. It is well known that the light distribution in dense media

^{†1} ISIR, Osaka University
^{†2} MIT Media Lab

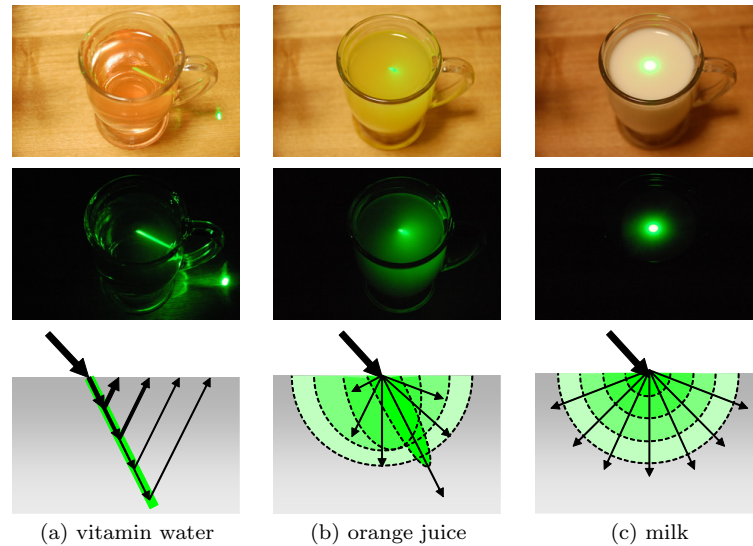


Fig. 3 Different scattering distributions.

becomes isotropic after incident rays undergo scattering many times as shown in Fig. 3 (c). This is called *diffusion approximation*. Stam⁴⁾ approximated the effects of multiple scattering in heterogeneous media. Jensen et al.⁵⁾ proposed an analytic dipole model based on diffusion approximation. The dipole model assumes that scatterings do not depend on the incident and radiative directions. It simulates subsurface light transport by locating a real positive light source under the surface and a virtual negative light source above the surface. Donner and Jensen⁶⁾ further extended this idea to render thin translucent slabs by multiple diffusion approximation. That is, multiple real positive light sources and virtual negative ones are located in such a way to satisfy the boundary condition. However, these methods cannot analyze the anisotropic distribution of lower-order scattering, such as 2- and 3-bounce scatterings.

Recently, Donner et al.⁷⁾ presented an empirical BSSRDF (bidirectional scattering surface reflectance distribution function) model to express directionally-dependent distributions. For example, both single and multiple scatterings are observed in orange juice as shown in Fig. 3 (b), and these generate a complex

light field. To handle this kind of general translucent object, the light transport for each bounce must be analyzed separately. Seitz et al.¹²⁾ proposed *inverse light transport* to decompose inter-reflections on the surface into individual bounce components, and we proposed a principle for bounce analysis of scattering lights¹³⁾.

Our contribution is similar to the inverse light transport, but we aim to analyze scattering light in translucent volumetric media. Although our method assumes that the target object is a homogeneous low-height 2-D volume for the sake of simplicity, a directionally-dependent distribution can be analyzed in detail by tracing multi-bounce scattering light. We introduce a new approach to predict recursively higher-order bounce scattering based on our fundamental analysis¹³⁾. We have added detailed analyses of frequency of the projected pattern, height of the target volume, and optical density of the target media. Moreover, we show that our separation method of single and multiple scatterings can be extended to 3-D volume media.

2. Related Work

Analysis based on dipole model: Since the dipole model can express the isotropic distribution of multiple scattering with a simple equation, it is used not only for rendering, but also in image analysis. For illumination, an arbitrary light environment⁸⁾, a focused narrow beam using a lens⁵⁾, a sweeping laser beam⁹⁾, a projector¹⁰⁾, or a fiber optic spectrometer¹¹⁾ is used to capture the image, and then the dipole model is fit. These methods can be applied only to optically dense media. In other words, the dipole or multipole model cannot be used for analyzing the anisotropic distribution of lower-order scatterings observed in optically thin media. Our method can treat anisotropic distribution by predicting multiple scatterings based on the light transport.

Face: Skin translucency has been the focus of much research. Tsumura¹⁴⁾ proposed a method to separate the hemoglobin and melanin components by independent component analysis, and estimated irradiance by the deconvolution of the point spread function of translucent media¹⁵⁾. More recently, the layered structure of skin has been analyzed and used for photo-realistic rendering^{16),17)}. None of these methods, however, assumes optically thin media.

Medical imaging: Interestingly, tomography in medical imaging deals with similar scattering problems^{18),19)}. Computational Tomography (CT) using x-rays can avoid most difficulties associated with light diffusion because x-rays go through the body without scattering. On the other hand, Diffuse Optical Tomography (DOT) using near-infrared light assumes that incident light diffuses in the body. Almost all DOT techniques assume that the diffusion is isotropic. Only a few methods attempt to use directionally-dependent distribution models based on the transport equation²⁰⁾. Our method differs from CT and normal DOT because we consider directionally-dependent distributions.

3. Light Transport Model in Scattering Media

3.1 Ray Scattering

In a scattering medium, the power of a ray is attenuated by repeated scattering. First, we have to model the attenuation of the scattering. **Figure 4** (a) illustrates the simple path of a ray emitted from point p_1 , scattered at point p_2 , and finally reaching point p_3 . According to the participating media theory⁴⁾, the power of the ray l_{p_3} at point p_3 can be modeled as

$$l_{p_3} = l_{p_1} \sigma_s p(\theta) e^{-\sigma_t(d_{12}+d_{23})}. \tag{1}$$

Here, l_{p_1} is the power of the ray at point p_1 , σ_s and σ_t are scattering and extinction coefficients of the media, respectively, and d_{12} and d_{23} are the distances between p_1 and p_2 and between p_2 and p_3 , respectively. The phase function $p(\theta)$ defines the asymmetry of the scattering distribution, and is approximated by

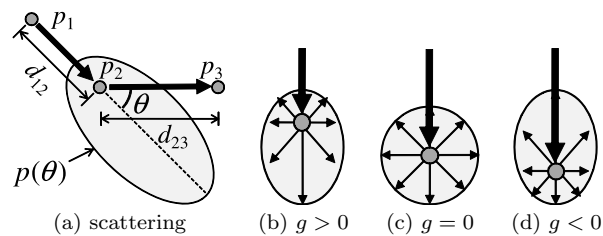


Fig. 4 Scattering model.

$$p(\theta) = \frac{1}{4\pi} \frac{1 - g^2}{(1 + g^2 - 2g \cos \theta)^{\frac{3}{2}}}. \tag{2}$$

Parameter g controls the shape of the distribution as shown in Figs. 4 (b)–(d). If g equals zero, the distribution becomes *isotropic*. A non-zero value of g corresponds to an *anisotropic* distribution, with positive and negative values called *forward-scattering* and *back-scattering*, respectively.

3.2 Components of a Light Field

The power distribution of all rays for each position and for each direction is expressed as a light field \mathbf{L} . The light field can be decomposed into individual bounce components. Let us assume that \mathbf{L}_0 is the light field directly generated by a light source as shown in **Fig. 5**. In a scattering medium, \mathbf{L}_0 is scattered once and generates a 1-bounce light field, \mathbf{L}_1 . The 1-bounce scattering is called a *single scattering*. Then the 1-bounce light field acts as an illumination and generates a 2-bounce light field, \mathbf{L}_2 . Similarly, a k -bounce light field, \mathbf{L}_k , generates a $(k + 1)$ -bounce light field, \mathbf{L}_{k+1} . A 2- or higher-order bounce scattering is called a *multiple scattering*. The complete light field in the medium is expressed as the sum of the individual bounce components, as

$$\mathbf{L} = \sum_{k=1}^{\infty} \mathbf{L}_k. \tag{3}$$

Light transport in a medium is represented by a light transport matrix, \mathbf{T} . The matrix describes how a ray from one point is propagated to other points, and can

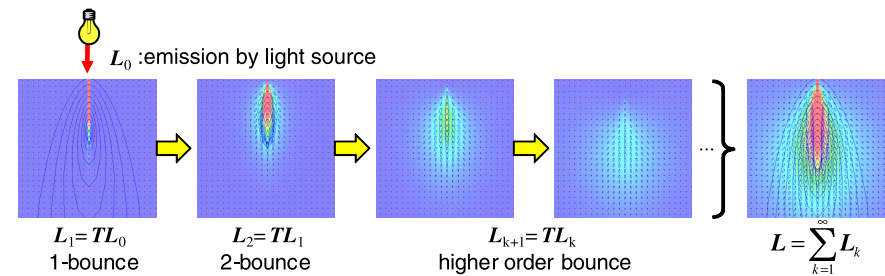


Fig. 5 Recursive propagation of a light field.

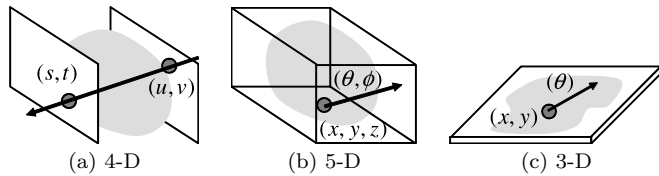


Fig. 6 Dimensions of a light field.

be calculated using Eq. (1), if parameters of the scattering medium are known. Using the light transport matrix, the 1-bounce light field corresponding to a single scattering is expressed as $L_1 = TL_0$. A 2-bounce light field is expressed as $L_2 = TL_1$. Similarly, a k -bounce light field is expressed recursively as

$$L_k = TL_{k-1}. \tag{4}$$

3.3 Dimensions of a Light Field

Now, we give a concrete definition of a light field. The light field in a volume can be expressed as a 4-D function. With two parallel planes sandwiching the volume, all rays can be defined using two coordinates (u, v) and (s, t) as shown in Fig. 6 (a). However, this definition assumes that the space is a vacuum and the power of the rays does not change along the path.

In a scattering medium, the power of the rays attenuates along the path. Hence, the light field should be expressed as a 5-D function of point (x, y, z) and direction (θ, ϕ) as shown in Fig. 6 (b). In general, a 5-D light field is difficult to handle and visualize because the data becomes extremely large.

If we limit the shape of the target object to a low-height volume such as a plate, the light field can be expressed as a 3-D function $l(x, y, \theta)$ of point (x, y) and direction (θ) . The light field vector L is defined as a series of this function, as

$$L = [l(0, 0, 0), \dots, l(W, H, 2\pi)]^T. \tag{5}$$

Here, W and H denote the width and height of the media, respectively.

In this paper, assuming a 2-D volume and a 3-D light field function, we fully analyze light transport in scattering media.

3.4 Light Field and Observed Image

We assume that a camera observes intensities over the surface of the target 2-D

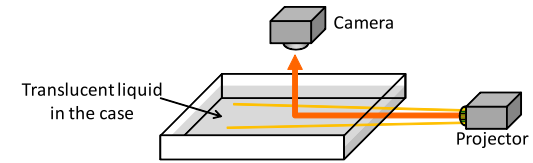


Fig. 7 Placement of the camera and projector.

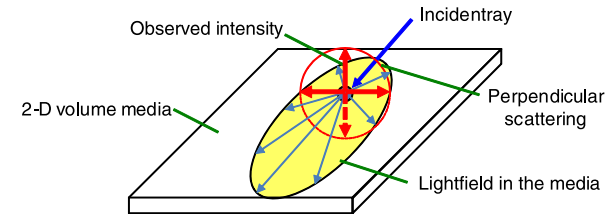


Fig. 8 Light field and observed image.

volume as shown in Fig. 7, and captures an image, I , which can be decomposed into individual bounce scatterings by

$$I = \sum_{k=1}^{\infty} I_k. \tag{6}$$

However, each bounce image I_k is not a slice of the corresponding light field L_k . While the light field describes the distribution of rays in the 2-D media volume, the observed image is a collection of rays in the surface normal direction as shown in Fig. 8.

To associate the light field with the observed image, we utilize the *rotational symmetry* of the scattering light around the ray. The power of the scattering light in the perpendicular directions is uniform regardless of the rotational direction. In fact, the observed brightness in the image is affected by the refraction index because the rays pass from the medium to air²¹⁾. Although we do not know the refraction index of the medium, the power of the rays and the observed brightness are proportional and the ratio is constant. That is, the relative intensities in the image can be calculated by Eq. (1) with $\theta = \pi/2$ up to the scale. Hence, both L_{k+1} and I_{k+1} can be predicted from the k -bounce light field L_k , if the light transport matrix T is known.

4. Separation of Single and Multiple Scatterings

4.1 Principle

All the bounce components are mixed in a captured image. Since each component has its own spatial distribution, direct analysis of the mixed components is not easy. Hence, our first goal is to extract only the single scattering components. We propose a novel method to separate single and multiple scatterings using a projector.

Nayar et al.²²⁾ presented a simple and effective method to separate direct and global components by projecting 2-D high-frequency patterns on the target scene. In their original method, the direct component corresponds to diffuse and specular reflections, while the global component corresponds to indirect reflections such as inter-reflection.

Since we wish to separate single and multiple scatterings, we change the projected patterns to 1-D high-frequency stripes with alternate white and black pixels as shown in **Fig. 9**. Although regions corresponding to black pixels are not directly illuminated, the brightness is not zero due to the global components. The brightness of an unilluminated region is half that of the global components, since half the pixels are white in the projected stripe pattern. On the other hand, the brightness of an illuminated region is equal to the sum of that of the direct components and half that of the global components.

In this case, single scattering is the direct component since it is caused by 1-bounce in the media. That is, components of single scatterings are observed only in the illuminated regions. On the other hand, multiple scattering is the

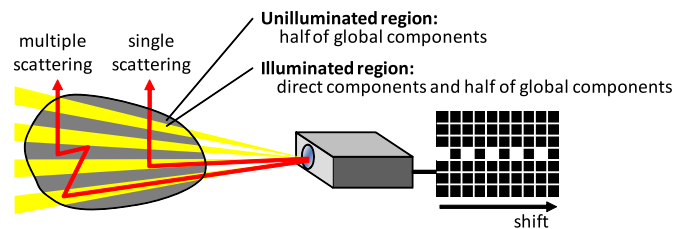


Fig. 9 Pattern projection of high-frequency stripes. By shifting the stripes, single and multiple scatterings are separated.

global component because it is observed regardless of the direct illumination from the projector. Hence, components of multiple scatterings are observed in both illuminated and unilluminated regions.

By shifting the 1-D high-frequency stripe pattern, several images are captured. The maximum and minimum intensities are observed for each pixel to generate images I_{\max} and I_{\min} , with the maximum and minimum intensities, respectively. Then, a single scattering image I_1 and a multiple scattering image I_M , corresponding to $\sum_{k=2}^{\infty} I_k$, are calculated by²²⁾

$$I_1 = I_{\max} - I_{\min}, \quad (7)$$

$$I_M = 2I_{\min}. \quad (8)$$

This allows us to separate single and multiple scatterings easily based on the same principle as in the high frequency illumination method²²⁾. The significant advantage is that it is not necessary to dilute the media to obtain single scattering components as required in Ref. 1).

4.2 Preliminary Experiments

As a preliminary experiment on separating single and multiple scatterings, we examined the frequency characteristic and its application. First, we analyzed the effects of the illumination frequency. We varied the width of the white pixels in the projected from 1 to 11 pixels in the captured image. **Figure 10** (a) shows the results for the various widths. The top and bottom rows show the separated single and multiple scatterings, respectively. The solid lines in Fig. 10 (b) show how the incident lights attenuate with distance from the incident point, while the broken lines show the results of fitting exponential functions. We can see that if the frequency of the projected pattern is too low, single and multiple scatterings cannot be well separated because the brightness of the multiple scatterings varies in local regions. As a result, the exponential function is not a good fit. Conversely, if the frequency is too high, it is difficult to distinguish illuminated and unilluminated regions using a camera, although the exponential function is a good fit. The reason is that projectors cannot faithfully project patterns with high frequencies because of defocus²³⁾ and imperfections in the optics²⁴⁾. That is, accurate blur analysis and radiometric analysis are necessary. Additionally, due to imperfect alignment of projector and camera pixels, the recorded amplitude of the pattern reduces for higher frequency patterns. As a result, single scatterings

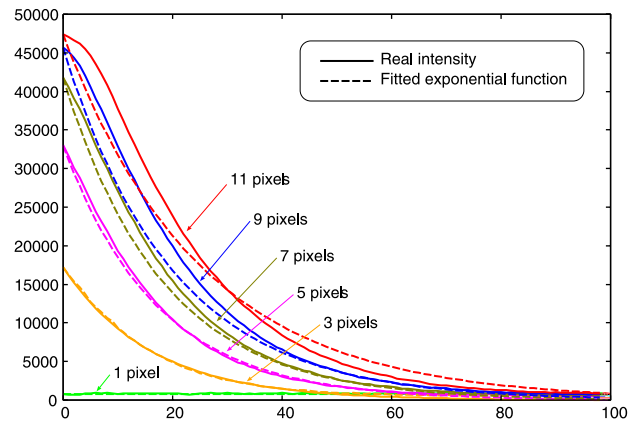
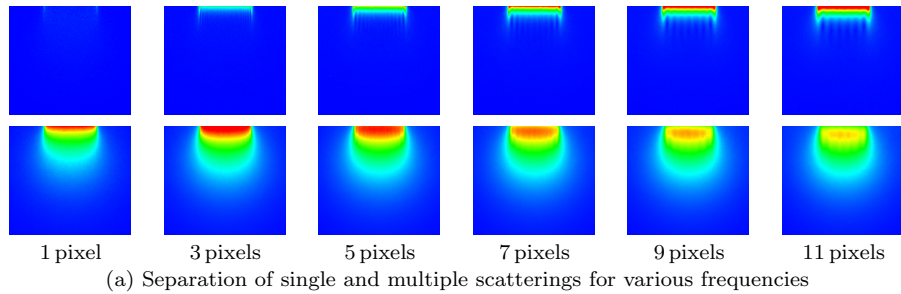


Fig. 10 Effects of illumination frequency.

are weakly observed. Hence, a suitable frequency does exist. According to this preliminary experiment, we found that the appropriate width for the white pixels is between three and five.

Next, we show that this separation method can be applied to 3-D inhomogeneous objects, although our analysis of scatterings is limited to 2-D low-height homogeneous media. By projecting 1-D stripe patterns, direct component including surface reflections as well as single scatterings and global component including multiple scatterings can be separated in a cross-section of the object. Hence, by repeating this process by sweeping the stripe patterns as shown in

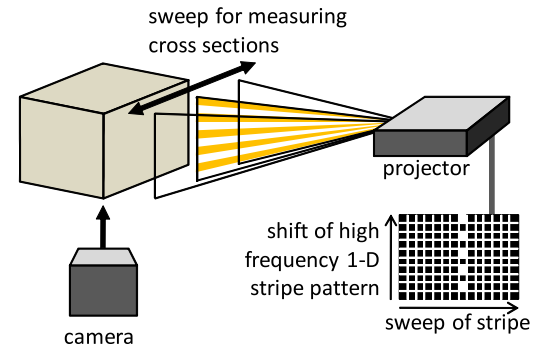


Fig. 11 Application to 3-D inhomogeneous object.

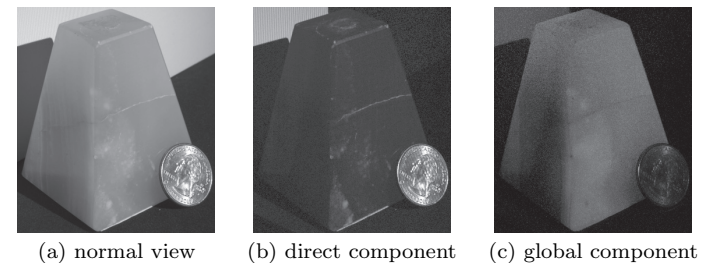


Fig. 12 Example of separation. The scene consists of marble and coin. Single scatterings and surface reflections are observed as the direct component, while multiple scatterings are observed as the global component.

Fig. 11, components in a 3-D volume can be separated. Figure 12(a) shows the target scene, which includes a marble and a coin, while Figs. 12(b) and (c) show the separated direct and global components, respectively. We can see that single scatterings in the marble and reflections on the marble and coin are observed as the direct component, while multiple scatterings are observed as the global component. Although single scattering is weak in Fig. 12(b) because this marble is optically dense, single and multiple scatterings in 3-D volume media can be separated by our method.

5. Analysis of Light Transport

5.1 Process Flow

The incident light to a translucent object repeats the scattering in the media and generates a complex light field. Our goal is to analyze how the incident light propagates in a scattering medium by tracing its light transport and visualize the light field for each bounce. Single and multiple scatterings can be separated by high-frequency stripe pattern projections as described in the previous section. Next, we analyze the single and multiple scatterings independently.

Figure 13 summarizes the analysis flow. First, single and multiple scatterings are separated. Then, the extinction parameter σ_t is estimated from the separated pure single scattering image. Next, multiple scattering is predicted from the light field of the single scattering by changing the parameters. Thus, the light field for each bounce scattering is estimated based on a forward rendering process. In the following sections, the detailed algorithms are discussed.

5.2 Analysis of Single Scattering

Single scattering is caused by one bounce of a ray between the light source

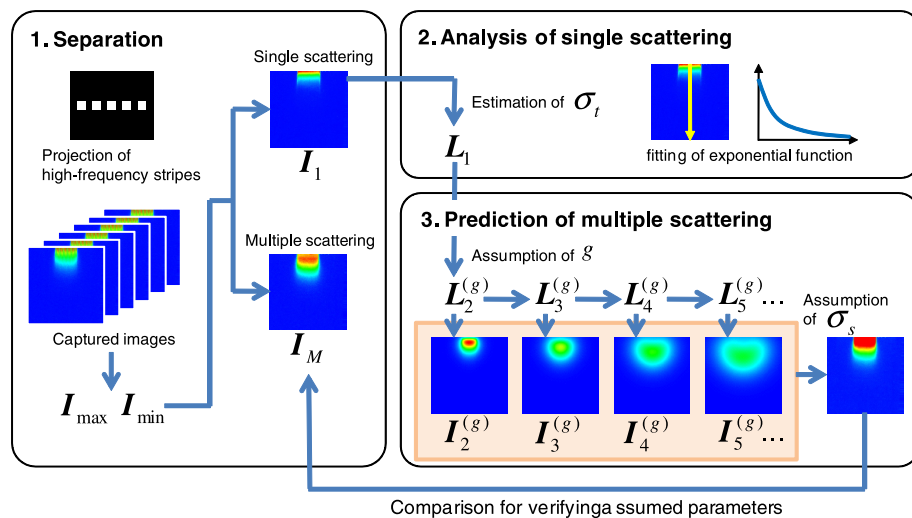


Fig. 13 Flow of analysis. Scattering parameters (σ_t , σ_s , and g) are estimated sequentially.

and the camera. Therefore, the path of the ray can easily be traced. Since the power of the light attenuates exponentially along the path, we fit an exponential function.

Let $s(d)$ be the intensity of I_1 at distance d from the incident point. Then, the extinction coefficient σ_t is estimated, so that the error between the exponential function and $s(d)$ is minimized by

$$\arg \min_{c, \sigma_t} \|s(d) - ce^{-\sigma_t d}\|_2. \quad (9)$$

Here, c is the scale parameter of the exponential function.

The light field L_1 generated by the single scattering is simple because rays from the light source go straight into the media with exponentially attenuating power. Hence, L_1 is easily estimated up to the scale factor.

5.3 Analysis of Multiple Scattering

Next, we recursively estimate the higher-order light fields corresponding to multiple scattering. At this point, the asymmetric parameter g and scattering coefficient σ_s are unknown. That is, the light transport matrix T , which is necessary to predict light fields, is also unknown. Hence, we estimate these parameters included in T based on a forward rendering process. However, our forward rendering is a unique two-step process that is optimized for bounce analysis.

In the first step, we render each bounce component separately without deciding the parameter σ_s . We temporarily assume $\sigma_s = 1$. Since the range of the asymmetric parameter is limited by $-1 \leq g \leq 1$, some candidates of the 2-bounce light field $L_2^{(g)}$ can be generated by changing parameter g . The higher-order (k -bounce) light fields $L_k^{(g)}$ and the corresponding images $I_k^{(g)}$ are recursively rendered according to the light transport equation, Eq. (1).

In the second step, the asymmetric parameter g and scattering coefficient σ_s are found so that the estimated higher-order component fits the real multiple scattering component I_M separated in Section 4. The concrete error is defined as

$$\arg \min_{\sigma_s, g} \|I_M - \sum_{k=2}^{\infty} \sigma_s^{k-1} I_k^{(g)}\|_2. \quad (10)$$

It should be noted that σ_s does not affect image $I_k^{(g)}$ or light field $L_k^{(g)}$, and is

only used as the weight of the linear combination of each bounce. Hence, two parameters can be estimated efficiently without simultaneously changing them.

Then, the light transport matrix \mathbf{T} is determined, and the complete light field \mathbf{L} is expressed as a linear combination of each bounce component, as

$$\mathbf{L} = \sum_{k=1}^{\infty} \sigma_s^{k-1} \mathbf{L}_k. \quad (11)$$

This analysis gives us the decomposed light fields and the light transport in the scattering medium.

This notion of a two-step rendering is useful because parameter σ_s can easily be changed after the first step via a relatively simple and fast linear combination of bounce component images. Computer graphics rendering methods do not allow post-synthesis parameter manipulation. We render each bounce independently, which means that we can easily modify the parameter through linear combination.

6. Experiments

6.1 Setup

Various experimental results for light transport analysis of real materials are presented in this section. We used diluted milk with water as the scattering medium as shown in **Fig. 14** (a) so that both single and multiple scatterings could be observed. The liquid is poured into a case painted matte black. Only a single side of the case is transparent so that the liquid can be illuminated from the side as shown in Fig. (b).

Since we assume that the target object is a low-height 2-D volume, the height of the liquid should be as low as possible. As a preliminary experiment, we changed the height and observed the distribution of scatterings. **Figure 15** shows the scatterings of an incident ray for various heights of the liquid. The incident height is about 2 mm below the top of the liquid. Obviously, the distribution changes as the depth of the liquid increases. However, if the height is less than 5 mm, it is difficult to illuminate the center depth correctly. Therefore, we set the height of the liquid to 5 mm.

Figure 14 (c) shows the setup for the measurements. A 3M MPro110 projector is positioned so as to illuminate the liquid in the case from the side, and a Point

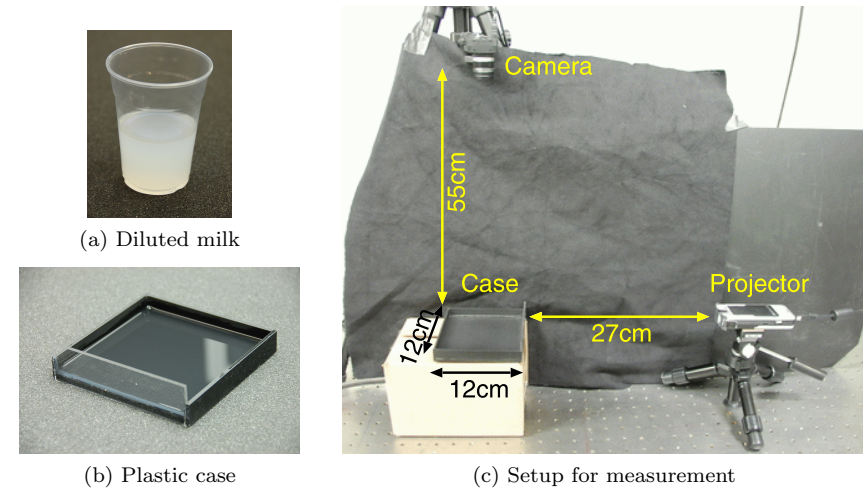


Fig. 14 Experimental setup.

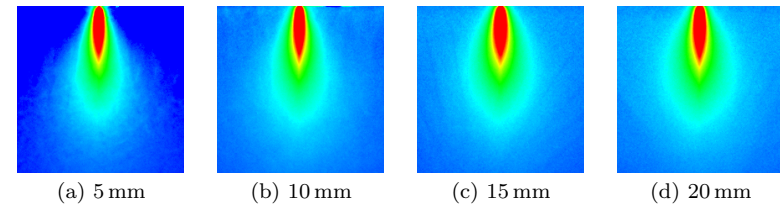


Fig. 15 The difference in scattering distribution with varying height of the liquid. Although the incident depths are the same, the distributions change due to 3-D paths of multiple scatterings.

Grey Chameleon camera is positioned above to capture images from the normal direction of the target plane.

6.2 Separation of Single and Multiple Scatterings

First, the single and multiple scatterings are separated. Six images are captured by shifting the high-frequency stripe pattern. **Figure 16** (a) shows one of the captured images, with the separated results shown in (b) and (c).

To evaluate the accuracy of the separated single scattering component, we compared the attenuation of the original intensity without separation with the

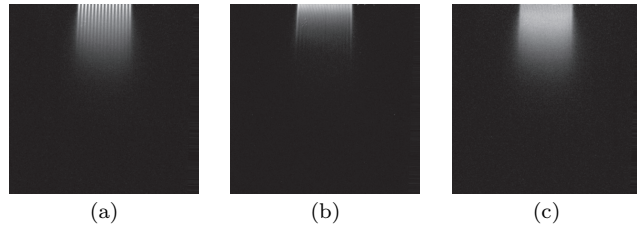


Fig. 16 Separation of single and multiple scattering components: (a) one of the captured images under high-frequency stripe illumination, (b) separated single scattering, and (c) separated multiple scattering.

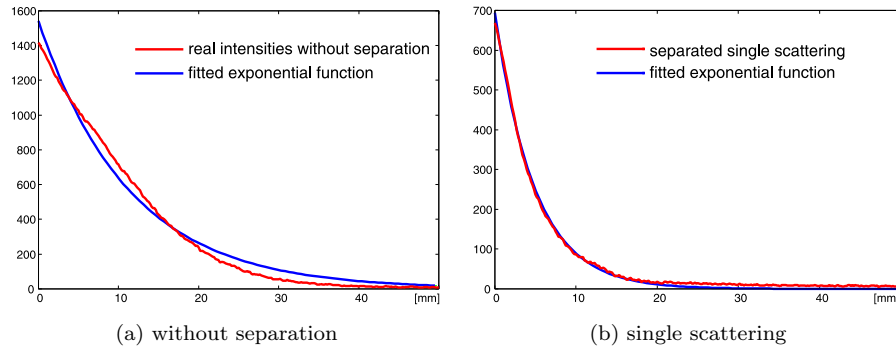


Fig. 17 Attenuation of incident illumination.

single scattering obtained by separation. **Figure 17** shows how the incident light attenuates with distance from the incident point. The red lines show the actual attenuation, while the blue lines show the fitting results of the exponential function. We can see that the exponential function does not fit the original intensity because it contains many higher-order scattering components. On the other hand, the exponential function fits the single scattering component well. We can see that the separated single scattering matches the light transport model and that the extinction coefficient can be estimated effectively. Based on this result, we estimated the value of σ_t as 0.2051, and obtained the light field of the single scattering.

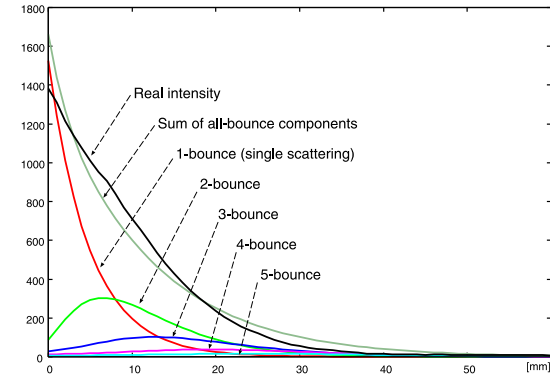


Fig. 18 Components of multiple scattering. Real intensities are decomposed into individual bounce scattering components. Higher-order components have peaks in the media with the peak positions moving inwards as the bounce order becomes higher.

6.3 Each Bounce Component of Light Field

Next, the most appropriate parameter set ($\sigma_a = 0.0366$ and $g = 0.4$) is estimated and the higher-order bounce components are calculated recursively. **Figure 18** shows how the incident light attenuates with distance from the incident point for each bounce component. We can see that the single scattering has a peak at the incident point and attenuates exponentially, while higher-order components have peaks in the media, and the peak positions move inwards as the bounce order becomes higher.

Finally, the light field for each bounce component is obtained as shown in **Fig. 19**. In this figure, the intensities are expressed in pseudo-color, while red '+' markers indicate the sampling points and blue ellipses indicate the angular distributions of the light field at the sampling point. We can see that the distribution of the lower-order bounce components have directional characteristics, while the distribution becomes isotropic as the bounce order becomes higher. These visualizations show how the incident ray repeats the scattering and the light is transported in the scattering medium.

Figure 20 illustrates another result in which the incident angle slants. The direction of the single scattering is the same as the incident angle, while the direction of a 2-bounce scattering is weakly affected by the incident angle. A

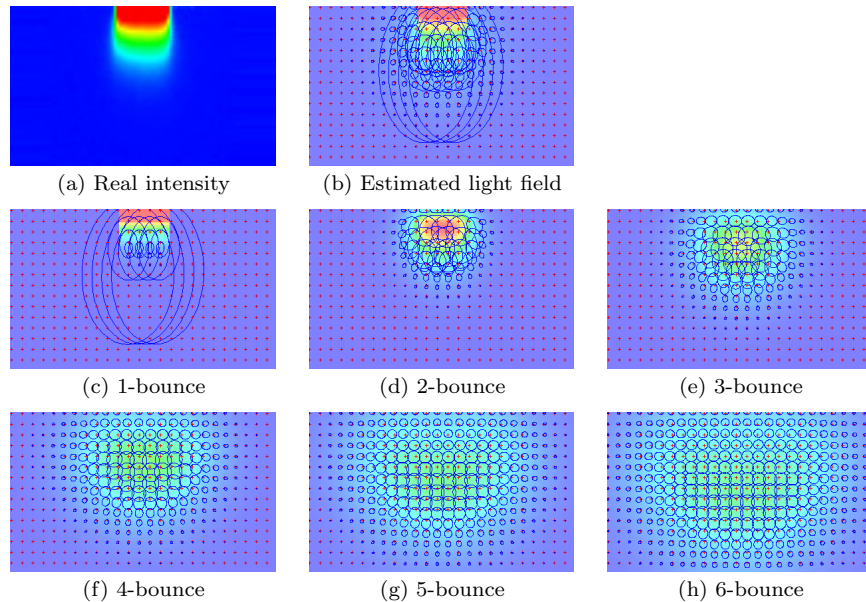


Fig. 19 Components of light field. The distributions of the lower-order bounce components have directional properties, while the distribution becomes isotropic as the bounce order becomes higher.

higher-order scattering becomes almost isotropic regardless of the incident angle.

7. Limitations

3-D light field: We assume that the target material has a low-height and that the light field can be described as a 3-D function. As discussed in Section 6.1, if a target object is a 3-D volume, all rays in the 3-D volume must be traced. Then, analysis, storage, and visualization become difficult.

Homogeneous material: Our method assumes that the scattering properties are uniform over the material. The process is divided into two steps. It is noted that the first step, separation of direct and global components, does not assume homogeneity. The only assumption is that the material varies smoothly. The second step, estimation of scattering parameters assumes homogeneity. Only for this step, dealing with inhomogeneous media would require more patterns, as in

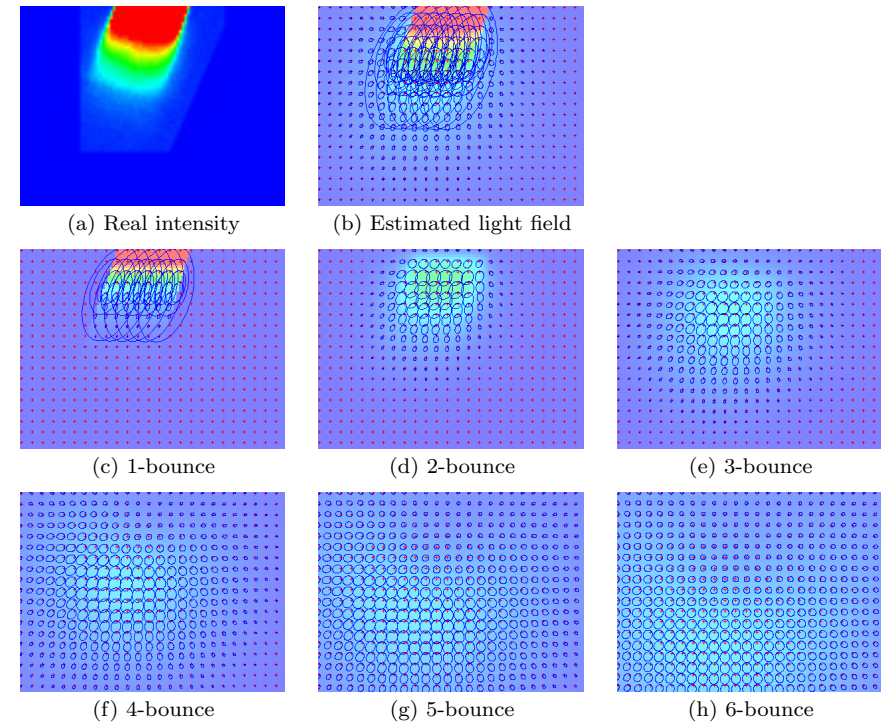


Fig. 20 Light fields of the slant incident illumination. Differences in directional properties are clearly observed.

CT.

Computational cost: In our method, scattering parameters are estimated within one second. However, the recursive calculation of a light field by Eq. (4) requires several hours, because all rays are traced exhaustively. To shorten the computational time, some faster methods such as Monte Carlo sampling may be applied.

Optical density of media: If optical densities of the target media are too dense, almost all of the observed lights become multiple scatterings. Single scatterings immediately attenuate at the incident point. **Figure 21** shows some examples of single and multiple scatterings that are separated by the proposed method.

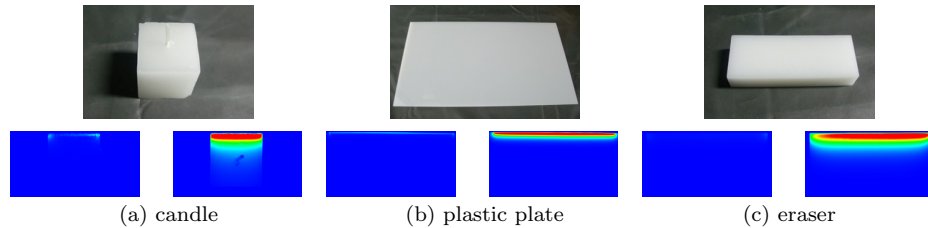


Fig. 21 Separation of single and multiple scatterings in optically dense media. Top row: target objects. Bottom row: the left and right images show the separated single and multiple scatterings, respectively. Since the single scatterings are too weak, our method cannot analyze optically dense media.

In optically dense media such as wax, plastic plates, and erasers, the separated single scatterings are too weak. Hence, these objects cannot be dealt with by the proposed method since our method predicts higher-order bounce scattering components from the single scattering.

8. Conclusion

We proposed a new method to decompose a light field for each bounce and visualize the light transport in a scattering medium. Multi bounce scattering is effectively analyzed in two steps. First, single and multiple scatterings are separated by projecting 1-D high-frequency stripe patterns. From the pure single scattering, the property of attenuation is stably estimated. Then, the multiple scattering is recursively decomposed into individual bounce components based on the light transport equation. Although the target object is limited to low-height, we believe that our method is a significant first step in analyzing light transport in translucent objects.

Our future work includes verification of the decomposed light transport. Since we do not know the ground truth, we cannot compare the results. We intend finding a relationship between the density of the liquid and the estimated parameters. Estimating the spatial distribution of the scattering parameters is also a future work, so that inhomogeneous material can be analyzed. As the number of unknowns increases, we may have to capture multiple images under changing illumination.

Acknowledgments This research is granted by the Japan Society for the Promotion of Science (JSPS) through the “Funding Program for Next Generation World-Leading Researchers (NEXT Program),” and by the Microsoft Research CORE5 project.

References

- 1) Narasimhan, S.G., Gupta, M., Donner, C., Ramamoorthi, R., Nayar, S.K. and Jensen, H.W.: Acquiring Scattering Properties of Participating Media by Dilution, *Proc. SIGGRAPH2006*, pp.1003–1012 (2006).
- 2) Gu, J., Nayar, S.K., Grinspun, E., Belhumeur, P.N. and Ramamoorthi, R.: Compressive Structured Light for Recovering Inhomogeneous Participating Media, *Proc. ECCV2008*, pp.845–858 (2008).
- 3) Hawkins, T., Einarsson, P. and Debevec, P.: Acquisition of Time-Varying Participating Media, *Proc. SIGGRAPH2005*, pp.812–815 (2005).
- 4) Stam, J.: Multiple scattering as a diffusion process, *Proc. Eurographics Rendering Workshop*, pp.69–79 (1995).
- 5) Jensen, H.W., Marschner, S.R., Levoy, M. and Hanrahan, P.: A Practical Model for Subsurface Light Transport, *Proc. SIGGRAPH2001*, pp.511–518 (2001).
- 6) Donner, C. and Jensen, H.W.: Light Diffusion in Multi-Layered Translucent Materials, *Proc. SIGGRAPH2005*, pp.1032–1039 (2005).
- 7) Donner, C., Lawrence, J., Ramamoorthi, R., Hachisuka, T., Jensen, H.W. and Nayar, S.: An Empirical BSSRDF Model, *Proc. SIGGRAPH2009*, pp.1–10 (2009).
- 8) Mukaigawa, Y., Suzuki, K. and Yagi, Y.: Analysis of Subsurface Scattering based on Dipole Approximation, *IP SJ TCVA*, Vol.1, pp.128–138 (2009).
- 9) Goesele, M., Lensch, H.P.A., Lang, J., Fuchs, C. and Seidel, H.P.: Disco – Acquisition of Translucent Objects, *Proc. SIGGRAPH2004*, pp.835–844 (2004).
- 10) Tariq, S., Gardner, A., Llamas, I., Jones, A., Debevec, P. and Turk, G.: Efficient Estimation of Spatially Varying Subsurface Scattering Parameters, *Vision, Modeling, and Visualization (VMV2006)*, pp.129–136 (2006).
- 11) Weyrich, T., Matusik, W., Pfister, H., Bickel, B., Donner, C., Tu, C., McAndless, J., Lee, J., Ngan, A., Jensen, H.W. and Gross, M.: Analysis of Human Faces using a Measurement-Based Skin Reflectance Model, *Proc. SIGGRAPH2006*, pp.1013–1024 (2006).
- 12) Seitz, S.M., Matsushita, Y. and Kutulakos, K.N.: A Theory of Inverse Light Transport, *Proc. ICCV2005*, pp.1440–1447 (2005).
- 13) Mukaigawa, Y., Yagi, Y. and Raskar, R.: Analysis of Light Transport in Scattering Media, *Proc. CVPR2010*, pp.153–160 (2010).
- 14) Tsumura, N., Ojima, N., Sato, K., Shiraishi, M., Shimizu, H., Nabeshima, H., Akazaki, S., Hori, K. and Miyake, Y.: Image-based Skin Color and Texture Analysis/synthesis by Extracting Hemoglobin and Melanin Information in the Skin, *Proc.*

- SIGGRAPH2003*, pp.770–779 (2003).
- 15) Tsumura, N., Usuba, R., Takase, K., Nakaguchi, T., Ojima, N., Komeda, N. and Miyake, Y.: Image-based control of skin translucency, *Proc. CGIV2006*, pp.8–11 (2006).
 - 16) Ghosh, A., Hawkins, T., Peers, P., Frederiksen, S. and Debevec, P.: Practical Modeling and Acquisition of Layered Facial Reflectance, *Proc. SIGGRAPH Asia 2008* (2008).
 - 17) Donner, C., Weyrich, T., d'Eon, E., Ramamoorthi, R. and Rusinkiewicz, S.: A Layered, Heterogeneous Reflectance Model for Acquiring and Rendering Human Skin, *Proc. SIGGRAPH Asia 2008* (2008).
 - 18) Boas, D.A., Brooks, D.H., Miller, E.L. and DiMarzio, C.A., Kilmer, M., Gaudette, R.J. and Zhang, Q.: Imaging the body with diffuse optical tomography, *IEEE Signal Processing Magazine*, Vol.18, No.6, pp.57–75 (2001).
 - 19) Gibson, A.P., Hebden, J.C. and Arridge, S.R.: Recent advances in diffuse optical imaging, *Phys. Med. Biol.* 50, R1-R43 (2005).
 - 20) Klose, A.D. and Hielscher, A.H.: Iterative reconstruction scheme for optical tomography based on the equation of radiative transfer, *Med. Phys.*, Vol.26, No.8, pp.1698–1707 (1999).
 - 21) Aronson, R.: Radiative transfer implies a modified reciprocity relation, *JOSA A*, Vol.14, No.2, pp.486–490 (1997).
 - 22) Nayar, S.K., Krishnan, G., Grossberg, M.D. and Raskar, R.: Fast Separation of Direct and Global Components of a Scene Using High Frequency Illumination, *Proc. SIGGRAPH2006*, pp.935–944 (2006).
 - 23) Gupta, M., Tian, Y., Narasimhan, S. and Zhang, L.: De (Focusing) on Global Light Transport for Active Scene Recovery, *Proc. CVPR2009*, pp.2969–2976 (2009).
 - 24) Holroyd, M., Lawrence, J. and Zickler, T.: A radiometric analysis of projected sinusoidal illumination for opaque surfaces, Technical Report, CS-2010-7, University of Virginia (2010).

(Received November 4, 2010)

(Accepted August 8, 2011)

(Released December 28, 2011)

(Communicated by *P.J. Narayanan*)



Yasuhiro Mukaigawa received his M.E. and Ph.D. degrees from University of Tsukuba in 1994 and 1997, respectively. He became a research associate at Okayama University in 1997, an assistant professor at University of Tsukuba in 2003, and an associate professor at Osaka University in 2004. He joined the MIT Media Lab as a visiting associate professor from 2009 to 2010. His current research interests include computer vision and computational photography. He is a member of IEICE, VRSJ, and IEEE.



Ramesh Raskar joined the MIT Media Lab from Mitsubishi Electric Research Laboratories in 2008 as head of the Lab's Camera Culture research group. His research interests span the fields of computational light transport, computational photography, inverse problems in imaging and human-computer interaction.



Yasushi Yagi is a professor at the Institute of Scientific and Industrial Research, Osaka university. He received his Ph.D. degree from Osaka University in 1991. After working at the Product Development Laboratory, Mitsubishi Electric Corporation, he joined Osaka University in 1990. The international conferences for which he served as the program/general chair include: ROBIO2006 (PC), ACCV2007 (PC), ACCV2009 (GC) and ACPR2011 (PC). He was an editor of IEEE ICRA CEB (2008–2011). He is an associate editor-in-chief of IPSJ Transactions on CVA. He has received several awards, including ACM VRST2003 Honorable Mention Award and PSIVT2010 Best Paper Award. He is a fellow of IPSJ and a member of IEICE, RSJ, and IEEE.